



## Thermomechanical properties of aluminum alkoxide (alucone) films created using molecular layer deposition

David C. Miller<sup>a,c,\*</sup>, Ross R. Foster<sup>a,c</sup>, Shih-Hui Jen<sup>b,c</sup>, Jacob A. Bertrand<sup>b,c</sup>,  
Dragos Seghete<sup>b,c</sup>, Byunghoon Yoon<sup>b,c</sup>, Yung-Cheng Lee<sup>a,c</sup>,  
Steven M. George<sup>b,c</sup>, Martin L. Dunn<sup>a,c</sup>

<sup>a</sup> Department of Mechanical Engineering, University of Colorado, Boulder, CO 80309, USA

<sup>b</sup> Department of Chemistry and Biochemistry, University of Colorado, Boulder, CO 80309, USA

<sup>c</sup> DARPA Center for Integrated Micro/Nano-Electromechanical Transducers (iMINT), University of Colorado, Boulder, CO 80309, USA

Received 1 April 2009; received in revised form 30 June 2009; accepted 6 July 2009

Available online 6 August 2009

### Abstract

Nanometer-scale-thick, polymer-like coatings deposited using the molecular layer deposition (MLD) technique constitute a new class of materials. The modulus and hardness of aluminum alkoxide (“alucone”) films grown using either homobifunctional or heterobifunctional reactants were measured using nanoindentation. Because the coatings are brittle and possess a significant tensile film stress immediately after deposition, the influence of film stress on the indentation measurements was quantified using a numerical analysis protocol. The film stress and coefficient of thermal expansion for alucone were determined using the wafer curvature method. Film stress was found to stabilize within the first thermal cycle, demonstrating a repeatable hysteresis thereafter. Curvature/time measurements on coated microcantilever beams indicated that the most significant evolution in film stress for alucone occurred during the initial 2 weeks of storage in the ambient environment. The temporal behavior is attributed to the change in thickness and/or modulus of alucone, and is consistent with the film stress becoming more compressive over time. An encapsulating alumina film, coated using the atomic layer deposition technique, was found to suppress the evolution of stress within alucone. The studies here suggest that the alucones have a greater elastic modulus than traditional polymers, are at present quite brittle and are prone to environmental influence. The MLD technique, however, possesses a rich wealth of options that enable the modulus, adhesion and chemical stability of the coatings to be tailored.

© 2009 Acta Materialia Inc. Published by Elsevier Ltd. All rights reserved.

**Keywords:** Thin film; Mechanical properties; Reliability; Durability; Robustness

### 1. Introduction

The atomic layer deposition (ALD) technique [1–4] may be used to grow thin metallic or ceramic films; the latter have found application as high  $\kappa$  dielectrics within the field of integrated circuit technology [5]. ALD coatings have been proposed to be utilized in a broad range of applications, including the encapsulation of compliant substrates [6,7], as well as the surface functionalization of nanoparti-

cles or nanotubes [8,9], porous films/membranes [9,10] and microsystems [11]. Such coatings may be used to tailor characteristics, including chemical permeation, charge dissipation, surface adhesion, corrosion sensitivity and tribological behavior [12].

In contrast, the recently developed technique known as molecular layer deposition (MLD) [13–17] may be used to create polymer-like films. MLD coatings might be utilized for the same purposes as ALD coatings. The different chemical species used in MLD may enable additional applications currently facilitated using traditional polymers, e.g. spatial patterning using photolithography. In addition, MLD may be interposed between ceramic layers, mechan-

\* Corresponding author. Tel.: +1 303 384 7855; fax: +1 303 384 6790.  
E-mail address: [dcm@colorado.edu](mailto:dcm@colorado.edu) (D.C. Miller).

## Report Documentation Page

*Form Approved*  
*OMB No. 0704-0188*

Public reporting burden for the collection of information is estimated to average 1 hour per response, including the time for reviewing instructions, searching existing data sources, gathering and maintaining the data needed, and completing and reviewing the collection of information. Send comments regarding this burden estimate or any other aspect of this collection of information, including suggestions for reducing this burden, to Washington Headquarters Services, Directorate for Information Operations and Reports, 1215 Jefferson Davis Highway, Suite 1204, Arlington VA 22202-4302. Respondents should be aware that notwithstanding any other provision of law, no person shall be subject to a penalty for failing to comply with a collection of information if it does not display a currently valid OMB control number.

1. REPORT DATE <b>JUL 2009</b>	2. REPORT TYPE	3. DATES COVERED <b>00-00-2009 to 00-00-2009</b>	
4. TITLE AND SUBTITLE <b>Thermomechanical properties of aluminum alkoxide (alucone) films created using molecular layer deposition</b>		5a. CONTRACT NUMBER	
		5b. GRANT NUMBER	
		5c. PROGRAM ELEMENT NUMBER	
6. AUTHOR(S)		5d. PROJECT NUMBER	
		5e. TASK NUMBER	
		5f. WORK UNIT NUMBER	
7. PERFORMING ORGANIZATION NAME(S) AND ADDRESS(ES) <b>University of Colorado, Department of Chemistry and Biochemistry, Boulder, CO, 80309</b>		8. PERFORMING ORGANIZATION REPORT NUMBER	
9. SPONSORING/MONITORING AGENCY NAME(S) AND ADDRESS(ES)		10. SPONSOR/MONITOR'S ACRONYM(S)	
		11. SPONSOR/MONITOR'S REPORT NUMBER(S)	
12. DISTRIBUTION/AVAILABILITY STATEMENT <b>Approved for public release; distribution unlimited</b>			
13. SUPPLEMENTARY NOTES			
14. ABSTRACT <b>Nanometer-scale-thick, polymer-like coatings deposited using the molecular layer deposition (MLD) technique constitute a new class of materials. The modulus and hardness of aluminum alkoxide (alucone) films grown using either homobifunctional or heterobifunctional reactants were measured using nanoindentation. Because the coatings are brittle and possess a significant tensile film stress immediately after deposition, the influence of film stress on the indentation measurements was quantified using a numerical analysis protocol. The film stress and coefficient of thermal expansion for alucone were determined using the wafer curvature method. Film stress was found to stabilize within the first thermal cycle, demonstrating a repeatable hysteresis thereafter. Curvature/time measurements on coated microcantilever beams indicated that the most significant evolution in film stress for alucone occurred during the initial 2 weeks of storage in the ambient environment. The temporal behavior is attributed to the change in thickness and/or modulus of alucone, and is consistent with the film stress becoming more compressive over time. An encapsulating alumina film, coated using the atomic layer deposition technique, was found to suppress the evolution of stress within alucone. The studies here suggest that the alucones have a greater elastic modulus than traditional polymers, are at present quite brittle and are prone to environmental influence. The MLD technique however, possesses a rich wealth of options that enable the modulus, adhesion and chemical stability of the coatings to be tailored.</b>			
15. SUBJECT TERMS			
16. SECURITY CLASSIFICATION OF:			17. LIMITATION OF ABSTRACT <b>Same as Report (SAR)</b>
a. REPORT <b>unclassified</b>	b. ABSTRACT <b>unclassified</b>	c. THIS PAGE <b>unclassified</b>	
			18. NUMBER OF PAGES <b>10</b>
			19a. NAME OF RESPONSIBLE PERSON



ically decoupling the layers, thereby increasing the critical strain associated with film cracking [18,19], while also creating a more tortuous path that limits the permeation of chemical species [20]. Both ALD and MLD coatings are expected to benefit from the characteristics unique to the deposition techniques, i.e. the resulting films are continuous, conformal, pinhole free and may be grown with sub-nanometer thickness control.

The mechanical properties, which have not been previously studied, are essential to the design and engineering of reliable components containing MLD films. Instrumented indentation [21,22] is a popular technique that has been employed to study a broad variety of thin film coatings. Properties, such as modulus and hardness, may be determined from the measured load vs. depth relationship for a prescribed tip impressed into a specimen. The mechanical response for a film is, however, only automatically decoupled from its host substrate at indentation depths that are significantly less than that of the film thickness [23]. Separately, owing to the limitations of the technique, including the tip (capability of its manufacture and wear related its use), the specimen (surface roughness, surface contamination, and alignment with respect to the tip) and the indent region (the evolution of its initial-geometry and -stress distribution), the indenter tip must typically be pressed into the specimen by at least 50 nm before the raw modulus and hardness measurements have stabilized [24]. For materials bearing a viscoelastic response, rapid indentation may be least subject to time-dependent variation, i.e. the modulus measurement may approach the instantaneous modulus [25]. The preferred method, however, is to maintain a constant maximum applied load before very rapidly unloading the specimen, whereupon the instantaneous modulus can be more assuredly determined [26]. In this method, the dynamic properties of the specimen material can also be evaluated during the “creep hold” at the maximum load [27,28].

The curvature of a film/substrate specimen is often used to examine the stress within the film as well as the coefficient of thermal expansion (CTE). Stoney's solution [29,30] relates the curvature to the stress in a thin film deposited on a thick substrate:

$$\sigma_f = \frac{E_s h_s^2}{6(1 - \nu_s) h_f} \Delta\kappa \quad (1)$$

For curvature vs. temperature measurements, CTE can be evaluated using the following equation [29,30]:

$$\Delta\kappa = \frac{6(1 - \nu_s) h_f E_f (\alpha_s - \alpha_f) \Delta T}{(1 - \nu_f) E_s h_s^2} \quad (2)$$

In these equations,  $\sigma$  represents stress (Pa),  $E$  the elastic modulus (Pa),  $h$  the thickness (m),  $\kappa$  the curvature ( $\text{m}^{-1}$ ),  $\nu$  the Poisson's ratio (unitless),  $\alpha$  the CTE ( $\text{ppm } ^\circ\text{C}^{-1}$ ) and  $T$  the temperature ( $^\circ\text{C}$ ). The subscripts f and s refer to the film and substrate, respectively. In practice, the uncoated substrate is not perfectly flat, therefore stress (Eq. (1))

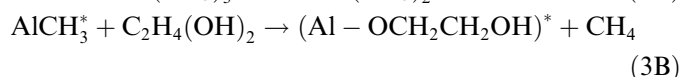
may be evaluated from the difference in  $R$ , the radius of curvature (m), present before and after deposition,  $\Delta\kappa = (\frac{1}{Ra} - \frac{1}{Rb})$ .

In the Stoney analysis, the film is assumed to be of uniform thickness, and  $\sigma_f$  is equibiaxial and constant throughout  $h_f$ . If  $h_f$  is not two orders of magnitude less than  $h_s$ , or for a stiff film on a compliant substrate, the system may be analyzed as a multilayer composite [31–33]. Such analysis is accurate and may be readily determined without a correction factor [33].

The goal of this study is to examine the basic thermomechanical properties of the recently developed alucone films, grown using the MLD technique. Specifically, the characteristics of elastic modulus, hardness, film stress and CTE are examined using indentation and the wafer curvature method. Drawing on the latter technique, temporal stability is also examined from the curvature of multilayer composite microcantilever beams. The examination here was motivated by the use of MLD to facilitate a chemical permeation barrier [19]; the results here are utilized in the study of the mechanical robustness of monolayer and multilayer composite coatings acting in that application.

## 2. Experimental

Films were deposited in a viscous flow reactor [4] using the MLD [13–17] technique. The technique does not require line-of-sight for deposition and films are deposited in blanket format. The deposition technique is based on a sequence of two or more self-limiting reactions between vapor-phase precursors and a solid surface. A simple recipe for aluminum alkoxide (“alucone”) film growth incorporates the two half-reactions, (3A) and (3B), where the asterisks designate the surface species [14]:



The reactants, trimethyl aluminum (TMA,  $\text{Al}(\text{CH}_3)_3$ ) and ethylene glycol (EG,  $\text{OHCH}_2\text{CH}_2\text{OH}$ ), are alternately injected via nitrogen carrier gas [14,15]. Using computer-controlled pneumatic valves, the substrate surface is first exposed to TMA, which reacts with the active surface sites (Fig. 1a). Then, after purging the by-products from reaction (3A), the surface is exposed to EG. This reaction regenerates the initial functional groups, preparing the surface for the next exposure to TMA (Fig. 1b). The film is grown to the desired thickness by repeating the AB sequence for “AB alucone”. The chemical growth represented in Fig. 1 is performed using homobifunctional reactants that may react twice with two separate chemical groups on the surface [15,16].

An MLD sequence using heterobifunctional and ring-opening reactants may be used to improve the growth rate by avoiding reactions with two separate chemical groups on the surface [15,16]. The reaction sequence utilized to

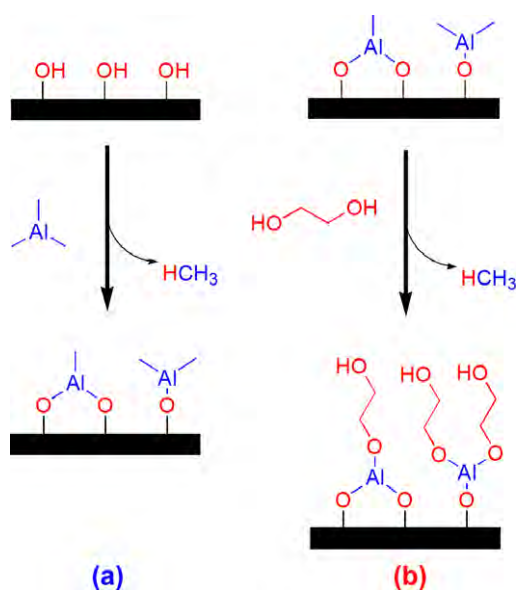


Fig. 1. The half-reaction sequence resulting in the growth of “AB alucone”. Film growth is realized according to the reactant sequence of (a) trimethyl aluminum and (b) ethylene glycol.

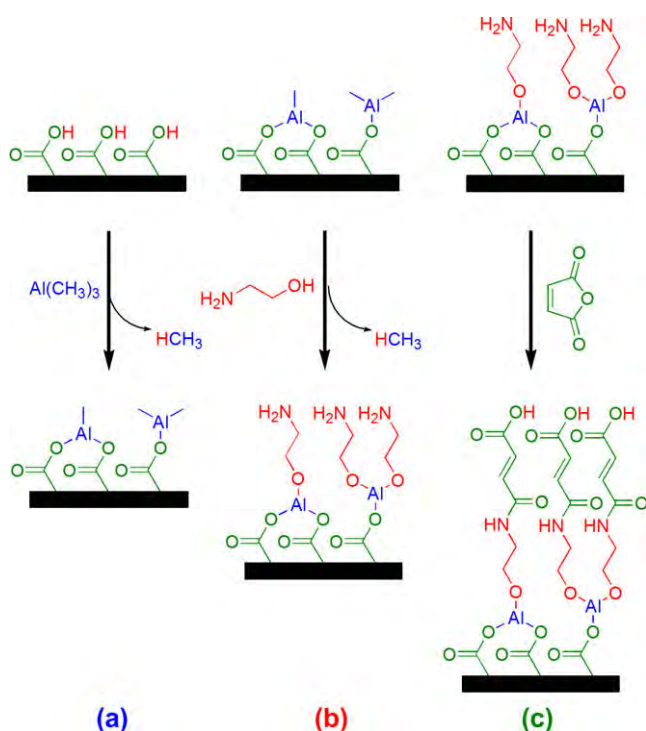
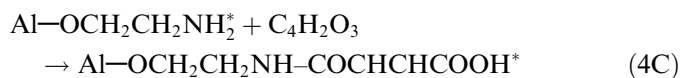
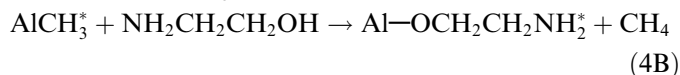


Fig. 2. Sub-reaction sequence resulting in the growth of “ABC alucone”. Film growth is realized according to the reactant sequence of (a) trimethylaluminum, (b) ethanolamine and (c) maleic anhydride.

grow “ABC alucone” [15] is represented in Fig. 2. Here, film growth proceeds according to the three reaction events, (4A)–(4C), where the initial reactant species are TMA, ethanolamine (EA,  $\text{NH}_2\text{CH}_2\text{CH}_2\text{OH}$ ) and maleic anhydride (MA,  $\text{C}_4\text{H}_2\text{O}_3$ ), respectively [15].



In the sequence, EA and MA act as heterobifunctional and ring-opening reactants, respectively, preventing “double” reactions at the surface. The reaction sequence is specifically enabled by the series of three surface events, thereby resulting in a constant rate of growth, as well as a more well-regulated molecular structure. AB alucone was grown at  $155^\circ\text{C}$ , whereas ABC alucone was grown at  $90^\circ\text{C}$ . Direct deposition, with no substrate surface treatment, was performed after a 12 h stabilization at the deposition temperature.

Indentation of alucone was performed at room temperature using a commercial instrument (Nano Dynamic Contact Module (DCM), Agilent Technologies, Inc.) equipped with a diamond Berkovich tip. When measured in “continuous stiffness” mode (CSM, Ref. [34]), modulus and hardness can be evaluated at discrete instances (unloading events) throughout the measured depth range. Once the tip has engaged the material’s surface, the instrument is capable of resolving load increments less than  $1\ \mu\text{N}$ , with displacement resolution less than  $1\ \text{nm}$ . The instrumented indentation method is accurate to within about 5–10% of the measured  $E$  and  $H$  values when multiple indentation measurements are averaged.

Specifics details of the indentation experiments are as follows: to prevent tip damage at high speed, the depth of indentation was set to be less than  $h_f$ . The test procedure followed the trapezoidal profile [22] by loading at the rate of  $25\ \mu\text{N s}^{-1}$ , holding at the maximum load for 180 s for stabilization, rapidly unloading at the rate of  $250\ \mu\text{N s}^{-1}$  and finally holding at 1% of the maximum load for 30 s to obtain a thermal drift correction. Test locations were offset by  $100\ \mu\text{m}$  to ensure isolation between the 30 separate sites.

Key details of the data reduction for the raw indentation measurements are as follows: immediately prior to the tests, the tip was calibrated against the elastic modulus of fused silica [21], with the area coefficients being chosen to achieve an optimum fit to the CSM data according to:

$$A[h_c] = \sum_{n=0}^4 C_n (h_c)^{2-n} = C_0 h_c^2 + C_1 h_c + C_2 h_c^{\frac{1}{2}} + C_3 h_c^{\frac{1}{4}} + C_4 h_c^{\frac{1}{8}} \quad (5)$$

In Eq. (5),  $A[h]$  represents the depth dependent area function ( $\text{m}^2$ ) and  $C$  the area fit coefficient(s). The contact depth,  $h_c$ , was determined according to a linear fit of the measured  $P$  vs.  $h$  data, just after the tip was unloaded:

$$h_c = h - \varepsilon \left. \frac{P}{S} \right|_{\text{unload}} \quad (6)$$

New parameters represented include  $h$ , which represents the measured depth (m),  $\varepsilon$ , the assumed sink-in parameter of 0.75 [21],  $P$ , the applied load (N), and  $S$ , the “harmonic

contact stiffness" (i.e.  $\partial P/\partial h$ ) ( $\text{N m}^{-1}$ ). The effective modulus was evaluated at the instant the tip was unloaded according to [21]

$$E_{\text{eff}} = \frac{S\sqrt{\pi}}{2\beta\sqrt{A[h_c]}} \Big|_{\text{unload}} \quad (7)$$

New parameters include  $E_{\text{eff}}$ , which represents the effective modulus (Pa),  $\pi$ , the mathematical constant, and  $\beta$ , the tip geometry factor – assumed to be 1.05 based on Ref. [35]. For the two-dimensional axisymmetric analysis, the effective modulus was related to the elastic modulus of the specimen using Eq. (8):

$$\frac{1}{E_{\text{eff}}} = \frac{1 - \nu_f^2}{E_f} + \frac{1 - \nu_i^2}{E_i} \quad (8)$$

In the equation, the subscripts  $f$  and  $i$ , refer to the film and the indenter tip, respectively.  $E_i$  and  $\nu_i$  were assumed to be 1141 GPa and 0.07, respectively, whereas  $\nu_f$  was assumed to be 0.33. The Berkovich hardness,  $H$ , was evaluated at the instant the tip was unloaded according to:

$$H = \frac{P}{A[h_c]} \Big|_{\text{unload}} \quad (9)$$

The raw load, depth and harmonic contact stiffness data were then utilized with a finite element analysis (FEA) protocol [36] that formally incorporates the effect of the substrate and allows for interpretation at shallow depths, i.e.  $\geq 20$  nm. Because the fused silica calibration (i.e. Eq. (5)) does not ensure a positive area of contact at shallow depths, the tip was assigned an ideal spherical shape for  $h \leq 2.5$  nm. For the (nonviscous) elastic/perfectly plastic constitutive behavior profile assumed here, the procedure works by interpolating the yield strength and modulus values from a fit of the simulated stiffness and force relative to those measured at a particular depth:

$$\sigma_y = a_1 S + b_1 P + c_1 \quad (10)$$

$$E = a_2 S + b_2 P + c_2 \quad (11)$$

$E$  and  $\sigma_y$  (therefore  $H$ ) are determined iteratively, from a set of initial guesses that bound the converged solution. To clarify, the parameter  $\sigma_y$  represents the yield strength of the film (Pa),  $S$  the harmonic contact stiffness ( $\text{N m}^{-1}$ ),  $P$  the applied load (N) and  $E$  the modulus of the film (Pa). To facilitate rapid analysis, the measurements were binned and averaged at twenty depths throughout the range of the experiment, where the fitting coefficients,  $a$ ,  $b$  and  $c$  are eliminated at each depth during the interpolation. In the protocol, an equibiaxial stress (constant through the thickness of the film) can be assigned during the FEA in order to examine the influence of  $\sigma_f$  on  $E$  and  $\sigma_y$  [36]. FEA was performed using a commercial code (ABAQUS, Dassault Systèmes Inc.) in conjunction with some custom front-end utilities and is described further in Refs. [36,37]. The values of  $E = 71.1$  GPa,  $\nu = 0.18$  and  $\sigma_y = 6635.4$  MPa were determined for the substrate, from an analysis of the fused silica calibration measurements; the value of  $\nu = 0.33$  was assumed for the alucone films.

AB alucone films, nominally 100 nm thick, were deposited on 300  $\mu\text{m}$  thick, 100 mm diameter (1 0 0) Si wafers (University Wafer, Inc.) for curvature measurements (FLX 2320-S, Toho Technology Corp.). Si substrates were utilized because the material is well characterized and is manufactured with high precision. The use of thin, large diameter wafers compensates the thickness and modulus of the alucone film (Eq. (1)). The FLX 2320-S measures radius of curvature based on the change in angle (incident vs. reflected) of a rastered laser. Linear scans ensure radius measurements to within 2.5% of the averaged value. The FLX 2320-S has a temperature controlled chuck, set here to record curvature at each  $5^\circ\text{C min}^{-1}$  increment. To prepare the specimens for measurement, alucone was removed from the backside of the wafer using highly basic ( $\text{pH} \sim 13$ ) solutions of NaOH (from pellets), hydrogen peroxide (30 wt.%) and deionized water. The coating dissolved readily when wiped with a solution-soaked tissue, visually verified by the indigo appearance of undissolved alucone. Before and after wafer curvature measurements, the film thickness and index of optical refraction were measured a small spot spectroscopic reflectometer (NanoSpec, Nano-metrics, Inc.).

Similar to the wafer curvature characterization, coatings were deposited on microcantilever beams in order to estimate film stress and monitor temporal stability. The microcantilevers consisted of laminated polycrystalline silicon (polySi),  $\text{SiO}_2$  and polySi layers, nominally 1.5, 0.3 and 1.0  $\mu\text{m}$  thick, respectively. Microcantilevers were fabricated on separate dice according to a standard microsystems technology (SUMMIT V, Sandia National Laboratories) [38]. Identical arrays of beams, each nominally 20  $\mu\text{m}$  wide, ranged in length from 100 to 550  $\mu\text{m}$  in 50  $\mu\text{m}$  increments. The microcantilevers were mechanically freed from sacrificial  $\text{SiO}_2$  layers by etching in a solution of 48 wt.% hydrofluoric acid (HF) and Triton-X 100 surfactant [39] for 20 min. The middle  $\text{SiO}_2$  layer of the beams is encased in Si, however, so that the  $\text{SiO}_2$  is not removed in HF. Other specific details of the microcantilever beams as well as the measurement technique are described more thoroughly in Ref. [37].

Because the beams are non-symmetric in the through-thickness direction, they exhibit an initial curvature of approximately  $-55 \text{ m}^{-1}$ . The curvature of the beams was measured using an interferometric microscope (New View 200, Zygo Corp.). The vertical resolution of the machine is better than 1 nm, while the lateral resolution for the 10 $\times$  objective at 0.75 $\times$  magnification is approximately 0.89  $\mu\text{m}$ . For the beams studied, the measurement accuracy of the instrument is therefore expected to be better than 1.2% (two standard deviations). Curvature was measured immediately before and after deposition, so that the stress in the coating can be determined using a multilayer composite analysis [31–33]. Curvature was then monitored weekly for 4 months.

The analysis procedure for the microcantilevers is formally described in Ref. [33]; the final step is to relate between microcantilever curvature and stress:

$$\Delta\kappa = \frac{(-B \cdot N) + (A \cdot M)}{(A \cdot D) - (B^2)} \quad (12)$$

New parameters in the equation include:  $A$ , the constant coupling axial extension between the layers (N);  $D$ , the bending coupling constant ( $\text{N m}^2$ );  $B$ , the constant coupling between extension and bending (N m);  $N$ , the term for the laminate force (N); and  $M$ , the term for the laminate bending moment (N m). The coefficients  $A$ ,  $B$  and  $D$  vary with the  $E$ ,  $\nu$  and  $h$  of each of the component layers. The terms  $N$  and  $M$  vary with the  $E$ ,  $\nu$ ,  $h$ ,  $\alpha$  and  $\sigma$  of the component layers, as well as  $\Delta T$ . Because the beam length was significantly greater than the width, the analysis was simplified to the one-dimensional condition, i.e. the layer width is eliminated.

### 3. Results

#### 3.1. Instrumented indentation

In post-examination, the far regions of the initial indentation specimens, 500 nm thick and deposited on Si, contained the “mud-crack” geometry commonly observed with equibiaxial tensile stress [40]. The indentation specific regions on these specimens also proved problematic as indentation resulted in cracking and delamination. Cracks can be analyzed according to Beuth’s model [41]:

$$G = \frac{\pi h_f (1 - \nu_f^2)}{2E_f} (\sigma_f)^2 g[D_1, D_2] \quad (13)$$

$$\Gamma = \frac{K_{IC}^2}{E_f} \quad (14)$$

New parameters in the equations include:  $D$ , which represents the Dunder’s parameters (unitless) [40];  $G$ , the energy release rate ( $\text{J m}^{-2}$ );  $g$ , a coefficient accounting for elastic misfit between the film and substrate (unitless) [41];  $\Gamma$ , the critical energy release rate ( $\text{J m}^{-2}$ ); and  $K_{IC}$ , the mode I fracture toughness of the film ( $\text{Pa m}^{0.5}$ ). The minimally sufficient condition required for fracture is realized when Eqs. (13) and (14) first become equal, where an isolated channel crack will propagate spontaneously across the film. The stress required for crack propagation is estimated to be 220 MPa, i.e. 0.5% strain, from the indentation measured modulus ( $E_f = 36.8 \text{ GPa}$ , below), the mode I fracture toughness of  $0.17 \pm 0.02 \text{ MPa m}^{0.5}$  measured in Ref. [19] for AB alucone, and assumed parameter values ( $\nu_f = 0.13$ ,  $E_s = 161.8 \text{ GPa}$ ,  $\nu_s = 0.22$ ). To prevent cracking, subsequent indentation studies were conducted using thinner (i.e. more mechanically robust [19]) films deposited on  $\text{SiO}_2$  substrates, where  $E_s$  was better matched to  $E_f$ .

In the subsequent studies, the polymer-specific measurement methods proved unsuccessful. Although both transients stabilized within 180 s, the magnitude of viscoelastic behavior at the maximum applied load [27,28] was exceeded by that of thermal drift. Separately, rapid unloading [26] at rates between 250 and 2500  $\mu\text{N s}^{-1}$  rendered con-

sistent instantaneous modulus values for polyethylene naphthalate and polyimide sheet specimens (75 and 50  $\mu\text{m}$  thick, respectively) but not for the alucone films. Therefore, the examination of alucone was limited to traditional techniques, i.e.  $P$  vs.  $h$  profiles as well as CSM data – which do not account for possible viscoelastic behavior.

Binned and averaged indentation data are shown in Fig. 3, including the variation in  $P/S^2$  and load with indentation depth.  $P/S^2$  [42] is never observed to converge asymptotically for either alucone sample, indicating that the substrate significantly affects the response, therefore its influence must be incorporated in the data analysis to obtain accurate values of  $E$  and  $H$ . Separately, the slope of the  $P$  vs.  $h$  loading profile for AB alucone is observed to exceed that of ABC alucone, indicating that AB alucone is a harder material.

The residual indentation impressions were imaged using a field-emitting scanning electron microscope (JSM-7401F, JEOL Ltd.). After a trace Au/Pd coating was applied to improve imaging capability, seven separate indentation sites were examined for each alucone; representative examples are shown in Fig. 4. No cracks were observed at the impression sites or in the distant open regions, verifying the validity of the indentation data. The crack free morphology is consistent with the 2.25 $\times$  strength improvement predicted (Eqs. (13) and (14)) relative to the 500 nm thick specimens. In Fig. 4, the outline of the residual impression is observed to bow slightly outwards, indicating a minor pile-up and the absence of work hardening [21]. A more convex shape than that in Fig. 4 can be problematic [21,22], since the area of contact would be underestimated, causing  $E$  and  $H$  to be overestimated. For ABC alucone, a

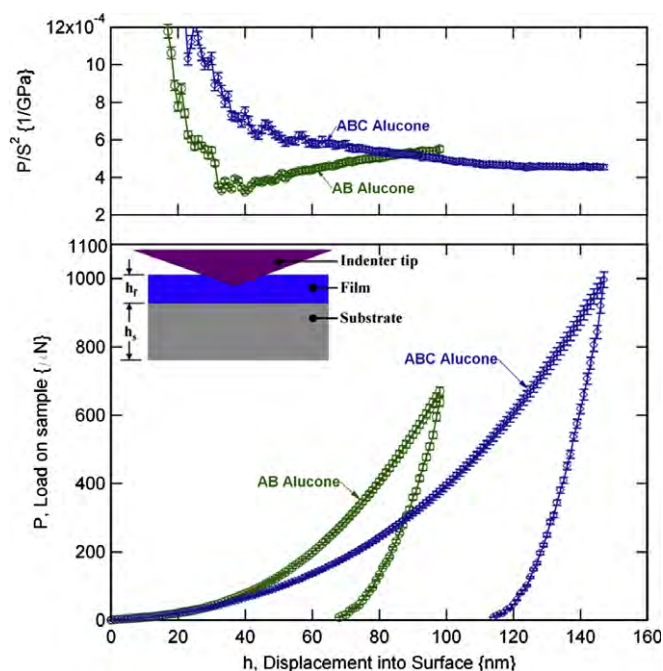
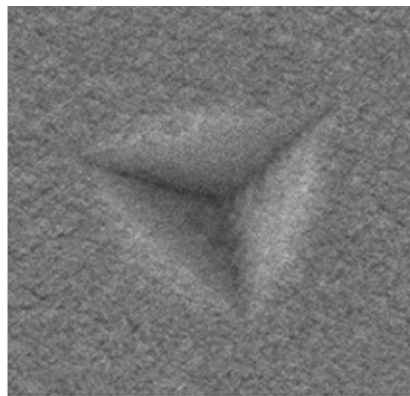
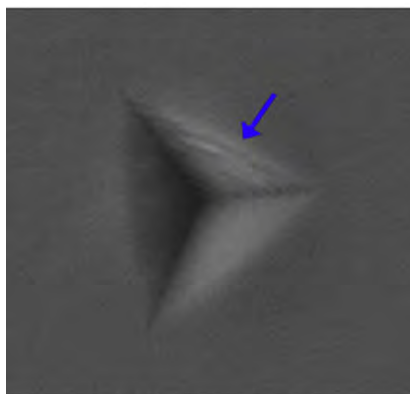


Fig. 3. Indentation results for 100 nm thick AB alucone and 120 nm thick ABC alucone films on  $\text{SiO}_2$ .



(a) — 200 nm



(b) — 400 nm

Fig. 4. Scanning electron images of the residual impression remaining after indentation for (a) 100 nm thick AB alucone and (b) 120 nm thick ABC alucone films on SiO<sub>2</sub>. The arrow identifies step-like features in the ABC sample.

step-like morphology was often observed on one of the impression faces, as indicated in Fig. 4b. This incremented geometry might relate to layers of alucone that are well adhered in the through-thickness direction.

The indentation data was then analyzed using the numerical analysis protocol [36]. First, AB alucone was evaluated up to just beyond to the critical stress for channel crack propagation (+441 MPa for the alucone/SiO<sub>2</sub> system via Eqs. (13) and (14); Fig. 5). To clarify,  $E$  and  $H$  in Fig. 5 were evaluated from the indentation data in Fig. 3 as a function of the  $\sigma_f$  that might be present; as described later,  $\sigma_f$  was independently verified to vary from tensile (+441 MPa) to compressive (−174 MPa) over time. As the fracture toughness of ABC alucone has not been measured, the indentation data was evaluated over the same range used for AB alucone (Fig. 6). In both figures, modulus is seen to vary monotonically; hardness, which further depends on inelastic material behavior, varies more complexly with stress. For reference, the characteristic values for  $\sigma_f = 0$  (dashed vertical lines in Figs. 5 and 6) are given in Table 1. The yield strength and corresponding strain,  $\varepsilon_y$ , are provided in the table for the assumed linear elastic limit.

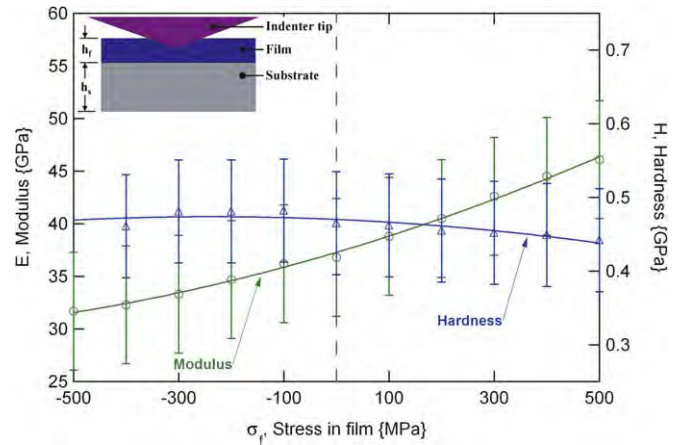


Fig. 5. Indentation results for the 100 nm thick AB alucone coating on SiO<sub>2</sub>. The variation in modulus and hardness with film stress was evaluated using the numerical analysis protocol for stresses in the range  $\pm 500$  MPa.

To begin discussion of the indentation results, Figs. 5 and 6 and Table 1 identify significant variation with  $\sigma_f$  over the range of  $\pm 500$  MPa. For AB alucone, a 14% and 7% variation with  $\sigma_f$  is observed for  $E$  and  $H$ , whereas for ABC alucone, a 33% and 57% variation with  $\sigma_f$  is observed for  $E$  and  $H$ , respectively. Regarding variation in  $H$  with  $\sigma_f$ , the  $\sigma_f$  limits assumed in the analysis are similar (84% and 113%, respectively) to the yield strength of alucone (Table 1). For a tensile film stress, for example, the material becomes more inclined to flow during indentation, decreasing its hardness. The geometry of the residual impression, which is accurately rendered in FEA, affects  $E$  through  $S$  as well as the corresponding area of contact (Eq. (7)).

Separate from the stress dependent variation, the uncertainty in the modulus measurements (Table 1) is due in part to the thickness of the films examined, i.e.  $h_f = 100$  or 120 nm. While the effect of the substrate is accurately represented in the numerical analysis, the associated uncertainty

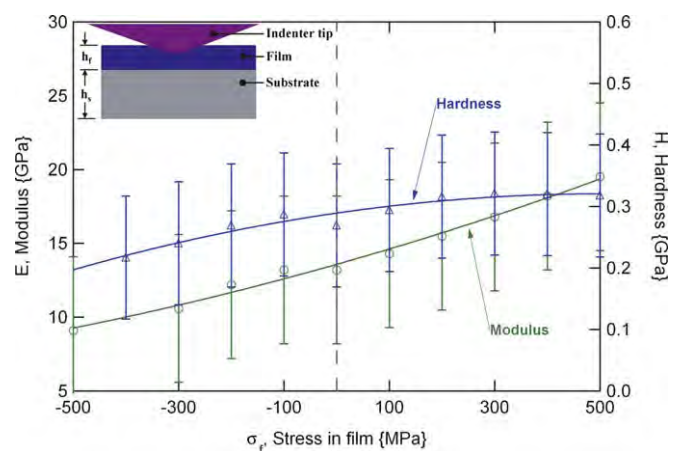


Fig. 6. Indentation results for the 120 nm thick ABC alucone coating on SiO<sub>2</sub>. The variation in modulus and hardness with film stress was evaluated using the numerical analysis protocol over the same stress range as for AB alucone.

Table 1

Summary of analysis results (average  $\pm 2$  SD) for the indented alucone films; the values for  $\sigma_f = 0$  are given.

Material	$E_f$ (GPa)	$H_f$ (GPa)	$\sigma_y$ (MPa)	$\varepsilon_y$ (%)
AB alucone	$36.8 \pm 5.6$	$0.47 \pm 0.07$	$596 \pm 91$	1.6
ABC alucone	$13.2 \pm 5.0$	$0.27 \pm 0.10$	$444 \pm 169$	3.4

is increased as  $h_f$  is decreased. The analysis, however, does not consider possible variation in  $\sigma_f$  between different deposition batches or according to the location on the substrate.

The yield strength and strain in Table 1 may be used to compare the mechanical capacity of the two alucone materials. The similar  $\sigma_y$  and  $\varepsilon_y$  values in the table suggest the toughness of ABC alucone is comparable to that of AB alucone. This is consistent with the mud-crack morphology observed for both 500 nm thick coatings, suggesting that both alucones are brittle.

While indentation enables rapid material characterization, the results here should be understood as initial estimates. The results of indentation are effectively isotropic, as the complicated three-dimensional strain field invoked does not readily distinguish anisotropic property variation [43,44]. In contrast to the measurement technique, the growth mechanisms depicted in Figs. 1 and 2 suggest that the MLD technique favors generating films bearing strong covalent bonds in the through-thickness direction, but with weak hydrogen bonds in the in-plane direction.

Separately, the effects of strain rate sensitivity, viscoelasticity and hydrostatic pressure are not emphasized in this study. First, indentation strain rates [45] as high as 0.018 and 0.012 s<sup>-1</sup> result from the loading rate of 25  $\mu\text{N s}^{-1}$  for AB and ABC alucone, respectively. In comparison, the strain rates of 0.75 and 0.63 s<sup>-1</sup> result from the CSM oscillations at the maximum  $h_c$ , respectively. While strain rate sensitivity was not directly examined, the indentation characterization occurs much more rapidly than in other situations, such as wafer- or microcantilever curvature characterization. Second, the thin films utilized here in order to prevent channel cracking are beyond the range of present equipment and methods related to viscoelasticity; therefore, the instantaneous  $E_f$  is approximated directly from  $E_{\text{eff}}$ , as mechanical dissipation is expected to be reduced at high strain rates. Third, particularly for polymeric materials, the hydrostatic pressure present during indentation can affect (increase)  $E_f$  and  $H_f$ . Material properties were extracted from  $h = 30$  to 50 nm and from  $h = 24$  to 108 nm for AB and ABC alucone, respectively, based on the uniform results at those depths. The constitutive model used in the analysis here, however, does not encompass the effect of hydrostatic pressure at indentation depths approaching the film thickness.

### 3.2. Wafer curvature

Fig. 7 shows the stress present in a nominally 100 nm thick AB alucone film, measured using the wafer curvature method in three consecutive thermal cycles, i.e. heating to

155 °C followed by cooling to the ambient. The initial stress value of  $-174 \pm 9$  MPa, present at the beginning of the first thermal cycle, was determined by comparing coated and uncoated wafers. During the first thermal cycle, stress remained relatively unchanged, except for the precipitous increase in compressive stress just prior to the return to ambient temperature (a similar response was observed in a separate specimen tested to 500 °C). The radius of curvature ranged from  $-48$  to  $-38$  m in the second and third thermal cycles, where the overlapping profiles demonstrate a repeatable hysteresis. Separate slopes were observed for the heating and cooling profiles, therefore separate least-squares fits are shown in Fig. 7. The fits, used with Eq. (2), identify the CTE to be  $12.6 \pm 0.6$  and  $7.1 \pm 0.3$  ppm °C<sup>-1</sup> for the heating and cooling profiles, respectively. A precipitous increase in compressive stress was observed at the end of second and third cooling cycles. In these samples, a 2.5 nm thick native oxide [46] is expected to be present at the interface between alucone and Si. This interlayer is, however, expected to have negligible influence here, as the interlayer is symmetric (present on both the top and bottom Si surfaces), and is significantly thinner than  $h_f$ .

Material stabilization occurring during the first thermal cycle is common in thin films, and is often motivated by the mechanisms of grain growth, recrystallization or (inter-/intra-) diffusion [47–49]. In the case of polymeric materials, mechanisms including outgassing, desorption, densification, phase transformation, material decomposition and crosslinking may also contribute to stabilization. Thin films typically become stabilized as long as subsequent thermal cycles do not exceed the previously used temperature- or time conditions [47–49]. Regarding prolonged measurements, one must be aware of creep (or other viscoelastic behavior) occurring at elevated temperature conditions [48]. In Fig. 7, the similarity between the second and third cycles suggests the alucone has stabilized, at least over the time scale of the experiment. The cause of the hysteresis occurring in those cycles is unknown and may be due to

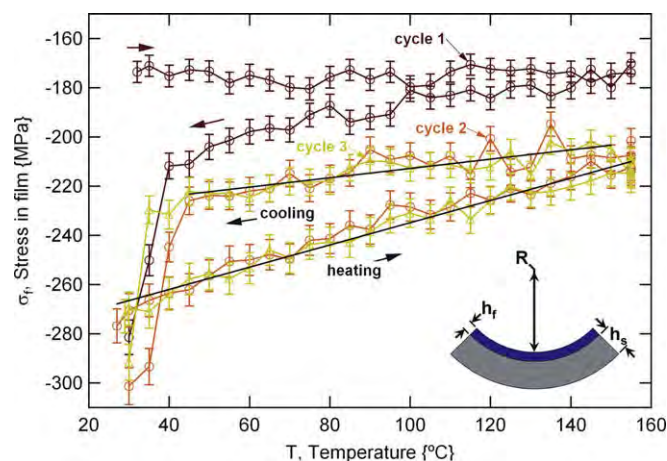


Fig. 7. Stress results, obtained using the wafer curvature method, over the first three consecutive thermal cycles for 100 nm AB alucone deposited on Si.

a phase transformation activated at elevated temperature, with the original characteristics being recovered near the ambient. The hysteresis might result from viscoelasticity and/or heat transfer (the thermal time constant).

Estimates of CTE, obtained from wafer curvature measurements, allow the contribution of thermal stress to be evaluated. The values of  $E_f = 36.8$  GPa,  $\nu_f = 0.33$ ,  $h_f = 85.5$  nm,  $E_s = 161.8$  GPa,  $\nu_s = 0.22$ ,  $h_s = 300$   $\mu\text{m}$  and  $\alpha_s = 3.0$  ppm  $^\circ\text{C}^{-1}$  were used in Eq. (2) to estimate the change in  $\sigma_f$ . For the maximum CTE of 12.6 ppm  $^\circ\text{C}^{-1}$ , the added tensile stress of 71.3 MPa is predicted for AB alucone, for the cooling from the deposition temperature to ambient temperature. In comparison, Eqs. (13) and (14) suggest that an absolute tensile stress of 441 MPa is required to crack the alucone/SiO<sub>2</sub> system in Fig. 5, for  $E_f = 36.8$  GPa,  $\nu_f = 0.33$ ,  $K_{IC} = 0.17$  MPa m<sup>0.5</sup>,  $E_s = 72$  GPa and  $\nu_s = 0.18$ . The tensile stress of 355 MPa was measured for alucone immediately after deposition using microcantilevers (below). The contribution of thermal misfit is therefore estimated to range from 1/5 to 1/3 of the initial  $\sigma_f$ , where the remaining stress is attributed to other factors, such as film growth. The parameters of temperature and pressure readily affect the rate of growth [14,17], and might also be used to manipulate  $\sigma_f$ .

Thermal cycling also affected other characteristics of AB alucone. While the nominal deposited thickness of alucone was 100 nm, the thickness just prior to the curvature characterization measured at 85.5 nm in the reflectometer. To clarify, curvature characterization was performed 2 weeks after film deposition for logistical reasons, including the removal of the coating present on the backside of the wafers. At the end of the wafer curvature experiments, the  $h_f$  had decreased further to 55.2 nm. The index of refraction,  $n$ , for alucone, also measured using the reflectometer, changed from 1.471 (just prior to thermal cycling) to 1.418 after the third cycle.

The decreases in  $h_f$  and  $n$  here are similar to those observed in a previous study. Specifically, a 22% decrease in thickness occurring within 5–6 days at ambient laboratory conditions was measured using X-ray reflectivity [14], which was observed along with change in chemical composition measured using Fourier transform infrared spectroscopy (FTIR) and X-ray photoelectron spectroscopy (XPS). The FTIR and XPS measurements indicate a change in the chemical composition of alucone, affecting  $E_f$ . The decrease in  $n$  (from 1.512 just after deposition to 1.494) also determined in Ref. [14] suggests a change in physical structure over time. The affected characteristics imply that the film stress of  $-174$  MPa measured at the beginning of the first cycle in Fig. 7 may not be present immediately after deposition. Therefore, the temporal stability of alucone was examined next.

### 3.3. Temporal stability (microcantilever curvature)

Separate coatings, including AB alucone nominally 100 nm thick, ALD Al<sub>2</sub>O<sub>3</sub> nominally 100 nm thick and a

laminated composite of Al<sub>2</sub>O<sub>3</sub>/AB alucone/Al<sub>2</sub>O<sub>3</sub> (nominally 25/192/25 nm thick), were grown on separate arrays of polySi/SiO<sub>2</sub>/polySi microcantilever beams. A representative micrograph of the microcantilever arrays is shown in the inset of Fig. 8, where the direction of positive curvature occurs for tip deflection towards the substrate. For the microcantilevers of known thickness (above), the parameters of  $E_f = 36.8$  GPa,  $\nu_f = 0.33$ ,  $h_f = 100$  nm,  $\alpha_f = 12.6$  ppm  $^\circ\text{C}^{-1}$ ,  $E_{\text{Si}} = 161.8$  GPa,  $\nu_{\text{Si}} = 0.22$ ,  $\alpha_{\text{Si}} = 3.0$  ppm  $^\circ\text{C}^{-1}$ ,  $E_{\text{SiO}_2} = 72.0$  GPa,  $\nu_{\text{SiO}_2} = 0.18$ ,  $\alpha_{\text{SiO}_2} = 0.4$  ppm  $^\circ\text{C}^{-1}$  and  $\Delta T = 125$   $^\circ\text{C}$  were used in Eq. (12) to estimate  $\sigma_f$ . For the analysis, the residual stress in the polySi layers was determined to be  $-2.8$  and  $-4.3$  MPa, respectively, using the pointer structure and procedure described in Ref. [50], whereas stress in the SiO<sub>2</sub> layer was assumed to be 0. From the difference in curvature prior to coating (arrows in Fig. 8) and immediately after coating (starting at 0 in Fig. 8),  $\sigma_f$  was determined to be  $355 \pm 57$  MPa for alucone. The film stress within Al<sub>2</sub>O<sub>3</sub> ALD coatings of different thickness is examined elsewhere [37], whereas the analysis for the Al<sub>2</sub>O<sub>3</sub>/alucone/Al<sub>2</sub>O<sub>3</sub> coating may not be solved specifically ( $\sigma_f$  for three coating layers is unknown). In Figs. 7 and 8,  $\sigma_f$  is importantly assumed to be constant through  $h_f$ ; an additional through-thickness gradient would affect the wafer and microcantilever  $\sigma_f$  solutions.

The evolution of curvature is shown in Fig. 8, where the change with time occurs mostly within 2 weeks for 100 nm alucone, a similar duration to that observed in Ref. [14]. The change in curvature for the composite coating is not outside the range of experimental variability, but might occur over a more prolonged time period. The Al<sub>2</sub>O<sub>3</sub> coating, however, does not demonstrate a definite change in curvature. A significant amount of the variability for the coatings containing alucone is due to the surface roughness, where the overall variation increased from 2% of the average microcantilever curvature at the beginning of the experiment for all coatings to over 6% of average curvature at the end of the experiment for 100 nm alucone.

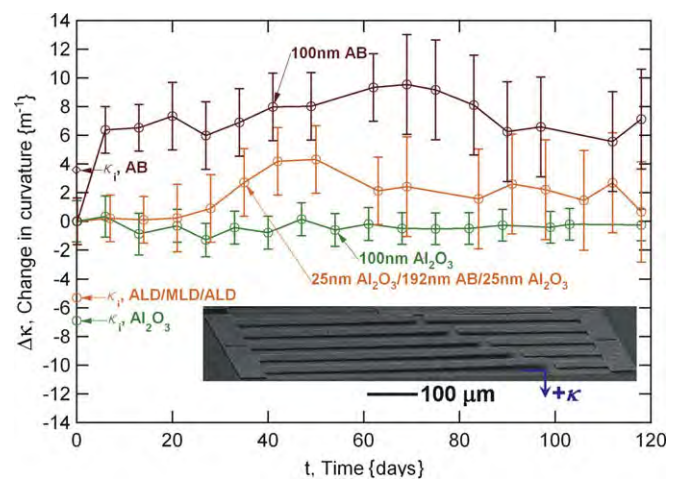


Fig. 8. Evolution of curvature over time for Si/SiO<sub>2</sub>/Si microcantilevers with alucone, Al<sub>2</sub>O<sub>3</sub> or Al<sub>2</sub>O<sub>3</sub>/alucone/Al<sub>2</sub>O<sub>3</sub> composite coatings.

The  $\sigma_f$  estimate of 355 MPa obtained from the microcantilevers is notably different from  $-174$  MPa, determined using wafer curvature.  $\sigma_f$  from the microcantilevers is, however, intermediate to the channel crack propagation stress estimated from Eqs. (13) and (14) for the indentation specimens ( $\sigma_f = 217$  MPa for  $h_f = 500$  nm, where cracking occurred, vs.  $\sigma_f = 441$  MPa for  $h_f = 100$  nm, with no cracking), suggesting that this value is reasonable. The tensile stress found immediately after deposition (as in Fig. 8) is consistent with the mud-crack geometry for  $h_f = 500$  nm, which cannot be explained if  $\sigma_f$  is compressive. The different stress values obtained from the wafer- and microcantilever-curvature measurements are therefore attributed to the evolving chemistry of alucone in the ambient environment.

Because both  $h_f$  and  $E_f$  change simultaneously with time, the change in  $\sigma_f$  over time in Fig. 8 cannot be determined absolutely. For a film of assumed constant thickness, however, the trend for the 100 nm alucone coated beams in Fig. 8 implies  $\sigma_f$  becoming more compressive over time. Such behavior is consistent with volumetrically additive processes, such as the incorporation of bulkier chemical species or rearrangement of molecular chains from the growth direction towards the in-plane direction. In Fig. 8, the  $\text{Al}_2\text{O}_3/\text{alucone}/\text{Al}_2\text{O}_3$  composite coating contains more alucone than the 100 nm thick coating, but does not significantly evolve over time. This stabilized behavior is attributed to the outermost  $\text{Al}_2\text{O}_3$  film, believed to prevent  $\text{H}_2\text{O}$  from diffusing into the interior films from the ambient environment. Similar behavior was seen in Ref. [14], where the properties of alucone were stabilized by an external coating. To explain, the interior alucone/ $\text{Al}_2\text{O}_3$  interface is believed to promote catalytically the dehydration and/or dehydrogenation of alucone when the alucone is not externally shielded from the environment [14]. In contrast, the 100 nm thick  $\text{Al}_2\text{O}_3$  coating did not change over time, within the range of experimental error.  $\text{Al}_2\text{O}_3$  ALD is believed to be much more chemically stable, except in extremely acidic or basic environments [14]. While ABC alucone was not examined here using reflectometry or microcantilever curvature, the initial study of that system in Ref. [17] also includes examination of temporal stability.

#### 4. Discussion

Many of the proposed applications for MLD involve replacing conventional polymeric materials with patterned MLD films for the purpose of miniaturization. The characterizations here suggest that the alucones have a greater elastic modulus than traditional polymers (Table 1 vs. Refs. [51,52]), are at present quite brittle (indentation and Ref. [19]) and are prone to environmental influence (Fig. 8 and Ref. [14]). Another issue of importance is the anisotropy of material properties, such as modulus and toughness. For example, in-plane measurements could be obtained via a pressurized MLD membrane or by bending an alucone coated microcantilever using an atomic force

microscope [53]. These techniques allow the rapid evaluation of the contribution of viscoelastic behavior, which was not investigated using the wafer curvature method and cannot be discerned from the chemistry motivated change in microcantilever curvature over time.

Beyond the characteristics measured here, the MLD technique provides considerable flexibility for tailoring thermomechanical characteristics. A wealth of chemical precursors may be utilized to increase the length of chemical chains, reorient the direction of growth, incorporate aromatic or other geometries, and/or promote bonding in the in-plane direction [15]. For example, reaction sequences with heterobifunctional or ring-opening reactants (Fig. 2) may readily promote chain alignment and material anisotropy. Contrary methods include the use of ultraviolet light or intermittent chemical precursors to affect chemical bond density, chain orientation and chain length. Tailoring of material characteristics might also be achieved through intermittent mixture with ALD chemistries in order to realize graded composite materials, constructed in monolayer increments [54].

#### 5. Conclusions

The thermomechanical properties of MLD alucone coatings were investigated using indentation, wafer curvature and microcantilever curvature measurements. Key results include the following:

For zero film stress, the elastic modulus of “AB” and “ABC” alucone was determined to be  $36.8 \pm 5.6$  and  $13.2 \pm 5.0$  GPa, respectively, while the Berkovich hardness of the same materials was  $0.47 \pm 0.07$  and  $0.27 \pm 0.10$  GPa, respectively. A 7–57% variation in modulus and/or hardness according to film stress was identified using a numerical analysis protocol. Minor pile-up was observed at the periphery of the residual indentation impressions, suggesting that the alucone materials do not undergo significant work hardening.

The coefficient of thermal expansion for AB alucone was determined to be  $12.6 \text{ ppm } ^\circ\text{C}^{-1}$  during heating and  $7.1 \text{ ppm } ^\circ\text{C}^{-1}$  during cooling using the wafer curvature method. The tensile thermal stress invoked during cooling from the deposition temperature to the ambient is therefore expected to be 70–90 MPa, i.e. 1/5–1/3 of the initial film stress. The stress present 2 weeks after deposition was  $-174 \pm 9$  MPa; this decreased to  $-280$  MPa following thermomechanical stabilization. Subsequent thermal cycles demonstrated a repeatable hysteresis. Both the thickness and index of refraction were reduced after thermal cycling.

Microcantilever-facilitated curvature studies identified a tensile film stress (estimated  $>300$  MPa), present immediately after deposition. Microcantilever curvature was found to evolve during the first weeks of storage in the ambient environment in conjunction with change in the thickness and/or modulus of the alucone coatings. The observed change in curvature is consistent with the film stress becoming more compressive over time. ALD surface coat-

ings were found to stabilize alucone within the ambient environment; alumina is believed to act as a permeation barrier, shielding alucone against moisture-induced changes. Beyond the properties measured here, the MLD technique possesses a rich wealth of options that enable the tailoring of the characteristics, adhesion and chemical stability of coatings composed of this new class of material.

### Acknowledgements

The authors are grateful to: Dr. James Knapp of Sandia National Laboratories, for his help with numerical analysis of indentation data; Mr. Fumio Kuruta and Dave Hurlbut of the Toho Technology Corporation, for the use of the FLX2320 wafer curvature instrument; and Arrelaine Dameron of the National Renewable Energy Laboratory, for feedback and discussion regarding the ALD and MLD techniques. This work was supported by WiSpry Inc. through the DARPA Center on Nanoscale Science and Technology for Integrated Micro/Nano-Electromechanical Transducers (iMINT) funded by DARPA N/MEMS S&T Fundamentals Program (HR0011-06-1-0048). This study is based upon work supported by the National Science Foundation under Grant No. IIP-0741177. Additional support was provided by the Air Force Office of Scientific Research.

### Supplementary material

Supplementary data associated with this article can be found, in the online version, at [doi:10.1016/j.actamat.2009.07.015](https://doi.org/10.1016/j.actamat.2009.07.015).

### References

- [1] Leskelä M, Ritala M. *Thin Solid Films* 2002;409:138.
- [2] Ritala M, Leskelä M. *Angew Chem Int Ed* 2003;42:5538.
- [3] Ott AW, Klaus JW, Johnson JM, George SM. *Thin Solid Films* 1997;292:135.
- [4] Elam JW, Groner MD, George SM. *Rev Sci Instr* 2002;73:2981.
- [5] Hong M, Kwo J. *ECS Trans* 2005;1:41.
- [6] Groner MD, George SM, McLean RS, Carcia PF. *Appl Phys Lett* 2006;88:051907.
- [7] Dameron AA, Davidson SD, Burton BB, Carcia PF, Scott McLean MR, George SM. *J Phys Chem C* 2008;112:4573.
- [8] Herrmann CF, Fabreguette FH, Finch DS, Geiss R, George SM. *Appl Phys Lett* 2005;87:123110.
- [9] Kim H, Lee HBR, Maeng W-J. *Thin Solid Films* 2009;517:2563.
- [10] Elam JW, Routkevitch D, Mardilovich PD, George SM. *Chem Mater* 2003;15:3507.
- [11] Herrmann CF, DelRio FW, Miller DC, George SM, Bright VM, Ebel JL, et al. *Sensors Actat A* 2007;135:262.
- [12] Hoivik ND, Elam JW, Linderman RJ, Bright VM, George SM, Lee YC. *Sensors Actat A* 2003;103:100–4.
- [13] Yoshimura T, Tatsuura S, Sotoyama W. *Appl Phys Lett* 1991;59:482.
- [14] Dameron AA, Seghete D, Burton BB, Davidson SD, Cavanagh AS, Bertrand JA, et al. *Chem Mater* 2008;20:3315.
- [15] George SM, Yoon BH, Dameron AA. *Acc Chem Res* 2009;42:498.
- [16] Adamczyk NM, Dameron AA, George SM. *Langmuir* 2008;24:2081.
- [17] Yoon B, Seghete D, Cavanagh AS, George SM. *Chem Mater*, submitted for publication.
- [18] Cordero N, Yoon J, Suo Z. *Appl Phys. Lett.* 2007;90:111910.
- [19] Miller DC, Foster RR, Zhang YD, Jen S-H, Bertrand JA, Lu ZX, et al. *J Appl Phys* 2009;105:093527.
- [20] Graff GL, Burrows PE, Williford RE, Praino RF. Gastric emptying of a nutritionally balanced liquid diet. In: Crawford GP, editor. *Proceedings of the second international conference on gastrointestinal motility*, November 1978. Hoboken, NJ: John Wiley & Sons; 2005.
- [21] Oliver WC, Pharr GM. *J Mater Res* 2004;19:3.
- [22] Fischer-Cripps AC. *Nanoindentation*. New York: Springer; 2002.
- [23] Menčík J, Munz D, Quandt E, Weppelmann ER. *J Mater Res* 1997;12:2475.
- [24] Miller DC, Talmage MJ, Gall K. *J Mater Res* 2006;21:2480.
- [25] Mencik J, Rauchs G, Bardon J, Riche A. *J Mater Res* 2005;20:2660.
- [26] Cheng YT, Ni W, Cheng CM. *J Mater Res* 2005;20:3061.
- [27] Fischer-Cripps AC. *Mater Sci Eng A* 2004;385:74.
- [28] Oyen ML. *Acta Mater* 2007;55:3633.
- [29] Stoney GG. *Proc Roy Soc A* 1909;82:172.
- [30] Ohring M. *Materials science of thin films*. San Diego (CA): Academic Press; 1992.
- [31] Jones R. *Mechanics of composite materials*. Philadelphia (PA): Taylor & Francis; 1999.
- [32] Clyne TW, editor. *Encyclopedia of materials: science and technology*, vol. 9. New York: Elsevier; 2001.
- [33] Dunn ML, Cunningham SJ, editors. *Handbook of nanotechnology*. New York: Springer-Verlag; 2006.
- [34] Joslin DL, Oliver WC. *J Mater Res* 1990;5:123.
- [35] Strader JH, Shim S, Bei H, Oliver WC, Pharr GM. *Proc Mat Res Soc Symp* 2005;841:R1.4.1.
- [36] Knapp JA, Follstaedt DM, Meyers SM, Barbour JC, Friedmann TA. *J Appl Phys* 1999;85:1460.
- [37] Miller DC, Foster RR, Jen S-H, Bertrand JA, Cunningham SJ, Morris AS, et al., in preparation.
- [38] Sniegowski JJ, DeBoer MP. *Annu Rev Mater Sci* 2000;30:299.
- [39] Miller DC, Boyce BL, Kotula PG, Stoldt CR. *J Appl Phys* 2008;103:123518.
- [40] Hutchinson JW, Suo Z. In: Hutchinson JW, Wu TY, editors. *Advances in applied mechanics*. San Diego (CA): Academic Press; 1992.
- [41] Beuth JL. *Int J Solids Struct* 1992;29:1657.
- [42] Page TF, Pharr GM, Hay JC, Oliver WC, Lucas BN, Herbert E, et al. *Proc MRS* 1998;522:53.
- [43] Vlassak JJ, Nix WD. *J Mech Phys Solids* 1994;42:1223.
- [44] Vlassak JJ, Ciavarella M, Barber JR, Wang X. *J Mech Phys Solids* 2002;51:1701.
- [45] Lucas BN, Oliver WC. *Metal Trans A* 1999;30:601.
- [46] Madou MJ. *Fundamentals of microfabrication: the science of miniaturization*. New York: CRC Press; 2002.
- [47] Gardner D, Flinn P. *Proc IEEE Trans Electron Dev* 1988;35:2160.
- [48] Keller RM, Baker SP, Arzt E. *Acta Mater* 1999;47:415.
- [49] Miller DC, Herrmann CF, Maier HJ, George SM, Stoldt CR, Gall K. *Thin Solid Films* 2007;515:3208.
- [50] Miller DC, Boyce BL, Dugger MT, Buchheit TE, Gall K. *Sensors Actat A* 2007;138:130.
- [51] Callister WD. *Materials science and engineering: an introduction*. Hoboken (NJ): John Wiley & Sons; 1996.
- [52] Meyers MA, Chawla KK. *Mechanical behavior of materials*. Upper Saddle River (NJ): Prentice Hall; 1999.
- [53] Prorok BC, Zhu Y, Espinosa HD, Prorok BC. Gastric emptying of a nutritionally balanced liquid diet. In: Daniel EE, editor. *Proceedings of the second international conference on gastrointestinal motility*, November 1978. Seattle (WA), New York: McGraw-Hill; 1979. p. 182–92.
- [54] Prorok BC, Zhu Y, Espinosa HD, Guo ZY, Bazant ZP, Zhao YF, et al. In: Nalwa HS, editor. *Encyclopedia of nanoscience and nanotechnology*. Los Angeles (CA): American Scientific Publishers; 2004.